⌘ *Author's Choice*

Formyl Peptide Receptors from Immune and Vomeronasal System Exhibit Distinct Agonist Properties*

Bernd Bufe[1,2], **Timo Schumann**[1,3], and **Frank Zufall**

From the Department of Physiology, University of Saarland School of Medicine, 66421 Homburg, Germany

Background: The role of formyl peptide receptors (Fprs) in the vomeronasal system remains unclear.
Results: Agonist properties of vomeronasal Fprs differ extensively from those expressed in immune cells.
Conclusion: We observe neofunctionalization of vomeronasal Fprs and functional conservation of immune Fprs.
Significance: These findings provide new insight into the sensory function and evolution of Fprs.

The formyl peptide receptor (Fpr) family is well known for its contribution to immune defense against pathogens in human and rodent leukocytes. Recently, several structurally related members of these receptors were discovered in sensory neurons of the mouse vomeronasal organ (VNO), key detectors of pheromones and related semiochemicals. Although the biological role of vomeronasal Fprs is not yet clear, the known contribution of other Fprs to host immune defense suggested that they could contribute to vomeronasal pathogen sensing. Precise knowledge about the agonist properties of mouse Fprs is required to determine their function. We expressed all seven mouse and three human Fprs using an *in vitro* system and tested their activation with 32 selected compounds by conducting high throughput calcium measurements. We found an intriguing functional conservation between human and mouse immune Fprs that is most likely a consequence of closely similar biological constraints. By contrast, our data suggest a neofunctionalization of the vomeronasal Fprs. We show that the vomeronasal receptor mFpr-rs1 can be activated robustly by W-peptide and structural derivatives but not by other typical ligands of immune Fprs. mFpr-rs1 exhibits a stereo-selective preference for peptides containing D-amino acids. The same peptide motifs are contained in pathogenic microorganisms. Thus, the ligand profile of mFpr-rs1 is consistent with a role in vomeronasal pathogen sensing.

The ability to detect molecular cues by nasal chemosensory cells is an essential feature in social recognition, whereby animals identify and recognize other individuals. In rodents, this process involves the capability to distinguish between infected and uninfected individuals (1), but the nature of the chemical cues and the underlying neuronal receptive mechanisms mediating sensory assessment of health status remain largely unclear. A detailed understanding of these questions at a molecular level is not only essential for gaining insight into mechanisms of chemical communication in animals, but should also contribute to understanding disease-related odors and diagnostic olfactory biomarkers in humans (2).

The rodent vomeronasal organ (VNO)[4] comprises an olfactory subsystem that plays an essential role in chemical communication (3–8) and, more recently, has also emerged as an interface between immune and nervous system function (9–11). Mouse vomeronasal sensory neurons (VSNs) express two large families of seven-transmembrane, G protein-coupled receptors, V1Rs and V2Rs: V1R-positive VSNs reside within the apical layer of the VNO epithelium, coexpress the G protein $G\alpha_{i2}$, and detect urine-derived small organic molecules related to physiological and endocrine status (5–8, 12). V2R-positive VSNs reside within the basal layer, coexpress $G\alpha_o$, and detect members of several extended peptide or protein families (7, 8, 12). These include peptide antigens that bind major histocompatibility complex (MHC) class I molecules (13), major urinary proteins (14), and exocrine gland-secreting peptides (15). Subsets of V2R-positive VSNs not only detect peptide ligands important for immune function, but they also express several immune-related molecules such as β_2-microglobulin and nonclassical MHC class 1b proteins (H2-Mvs or M10s) (16, 17).

Besides V1Rs and V2Rs, a third family of G protein-coupled receptors consisting of members of the formyl peptide receptor (Fpr) family has recently been discovered in some VSNs, providing yet another link between immune and vomeronasal system function (18, 19). Mouse VSNs express five distinct Fprs: one of these (*mFpr-rs1*) is coexpressed with $G\alpha_o$ whereas the remaining four genes (*mFpr-rs3*, *mFpr-rs4*, *mFpr-rs6*, and *mFpr-rs7*) are coexpressed with $G\alpha_{i2}$ (18, 19). These results are intriguing because Fprs are known to play important roles in host defense against pathogens by recognizing a broad spectrum of chemical attractants that are either secreted by invading pathogens or released during inflammatory processes (20, 21). For instance, prototypical ligands of human Fprs are N-terminally formylated peptides found in bacteria such as *N*-form-

---

⌘ *Author's Choice*—Final version full access.
[1] Both authors contributed equally to this work.
[2] To whom correspondence should be addressed: University of Saarland School of Medicine, Kirrbergerstr. Bldg. 58, 66421 Homburg, Germany. Tel.: 06841-16-26047; Fax: 06841-16-26655; E-mail: bernd.bufe@uks.eu.
[3] Recipient of a graduate scholarship (GradUS) from the University of Saarland.

[4] The abbreviations used are: VNO, vomeronasal organ; DMSO, dimethyl sulfoxide; FLIPR, fluorescence imaging plate reader; fMLF, *N*-formylmethionine-leucine-phenylalanine; Fpr, formyl peptide receptor; VSN, vomeronasal sensory neuron.

ylmethionine-leucine-phenylalanine (fMLF) (22, 23). Human FPRs (hFPRs) also interact with a variety of other peptides such as the antimicrobial CRAMP (24), the neuroprotective-acting humanin (25) or HIV envelope proteins (26), and even with some nonpeptide ligands, such as the inflammatory modulator lipoxin A4 (27). Therefore, it has been suggested that vomeronasal Fprs have an olfactory function that is associated with the identification of pathogens, or the social recognition of pathogenic states (18, 19).

Consistent with the expression of Fprs in VSNs, several typical ligands for immune Fprs have been shown to activate subsets of native VSNs. These include fMLF, CRAMP, and lipoxin A4 in one study (19) and fMLF and the mitochondrially encoded peptides NDI-6T and NDI-6I in another (28). However, there is currently no direct link between the activation of specific VSNs by formylated peptides and the expression of a given Fpr in these sensory neurons, and *in vitro* expression studies designed to identify vomeronasal Fpr agonists revealed divergent results. Whereas one study reported that fMLF activates the vomeronasal receptors mFpr-rs3, mFpr-rs4, mFpr-rs6, and mFpr-rs7 (19), others (18, 29, 30) did not observe any activation of these receptors despite using similar methods and fMLF concentrations. Therefore, further experimentation is required.

Here, we used an *in vitro* expression assay in combination with high throughput measurements of intracellular Ca^{2+} to compare the agonist properties of two immune and five vomeronasal Fprs from mouse with those of three human immune Fprs (Fig. 1*A*). By testing all 10 receptors with a selection of 32 potential ligands, we obtained several novel conclusions with respect to Fpr function. We identified W-peptide as an effective ligand for the vomeronasal receptor mFpr-rs1 and provided evidence that this receptor has a stereo-selective preference toward D-amino acid-containing peptides that exist in a variety of pathogenic bacteria, viruses, and fungi. These results open new perspectives for the function of the mammalian VNO in the social recognition of infected individuals.

EXPERIMENTAL PROCEDURES

Cloning of Fpr Genes—Human genes were cloned from genomic DNA. Mouse receptors were PCR-amplified from vomeronasal cDNA and genomic DNA of C57BL/6J mice using Phusion HF Master Mix (Thermo Scientific) according to manufacturer's protocols.

Primer sequences and annealing temperature were: ATG GAG ACA AAT CCC TCT CTC CC and CTT TGC CTG TAA CTC CAC CTC TGC, 65 °C for hFPR1; ATG GAA ACC AAC TTC TCC ACT CCT C and CAT TGC CTG TAA CTC AGT CTC TGC A, 65 °C for hFPR2; ATG GAA ACC AAC TTC TCC ATT CCT and CAT TGC TTG TAA CTC CGT CTC CTC, 65 °C for hFPR3; ATG GAC ACC AAC ATG TCT CTC CTC A and TTT CCT CAA TTG GAT ATC GCG GCC GCA AGA GC, 59 °C for mFpr1; ATG GAA TCC AAC TAC TCC ATC CAT CT and TGG GGC CTT TAA CTC AAT GTC TG, 64 °C for mFpr2; ATG GAA TCC AAC TAC TCC ATC CAT CT and TAT TGC CTT TAT TTC AAT GTC TTC AGG AAG T, 64 °C for mFpr-rs1; ATG GAA GCC AAC TCC TCC ATC and TAG

TTC AGA GTC GGC AGG ACA TGA, 64 °C for mFpr-rs3; ATG GAA GTC AAC ATT TCA ATG CCT CT, GTC TTC CCT CAG GGC CCT CTC and 64 °C for mFpr-rs4; ATG GAA GCC AAC TTC TCC ATA CCT C and GAG TCT TTG TGA AGA CAA GTT TCT G, 64 °C for mFpr-rs6; ATG GAA GCC AAC TTC TCC ATA CCT C and GAG TCT TAA GTT TGT GAA GAC AAG TTT CTG ATT T for mFpr-rs7. All forward primers contained an additional 5′ sequence AAA GAA TTC AAG CTT CCT GCA GGC GCC ACC in front of the start codon that includes restriction sites and a Kozak sequence. All reverse primers were fused with an additional 3′ sequence TTT CCT CAA TTG GAT ATC GCG GCC GCA AGA GCT CA carrying the stop codon and restriction sites.

For functional studies, all receptors were cloned into pcDNA3.1 (Invitrogen). For immunocytochemical analyses, all Fpr genes were inserted into a modified pcDNA5/FRT/TO (Invitrogen) vector and expressed as fusion proteins with 39 amino acids of bovine rhodopsin added to the N terminus of the receptors. Full coding regions of all receptors were sequenced. The mFpr-rs1 isoform isolated from vomeronasal cDNA corresponds to NM_008042.2. mFpr-rs3 and mFpr-rs6 are identical to NM_008040.2 and NM_177316.2, respectively. mFpr-rs4 corresponds to NM_008041.2 but has A69T and G577A exchange. mFpr-rs7 corresponds to AF437513 with T441G and T500C exchange. These deviations were also observed in genomic DNA of C57BL/6J mice. Human hFPR2 and hFPR3 correspond to NM_001462.3 and NM_002030.3, respectively; hFPR1 corresponds to NM_001193306.1 with a V111L, R163H, and N192K exchange.

Cell Culture and Transient Transfection—Cells were maintained until 80–90% confluence in DMEM with 4.5 g/liter glucose (Invitrogen) containing 5% heat-inactivated bovine calf serum (Biochrom), 10,000 units/ml penicillin G (Sigma), 10 mg/ml streptomycin and 2 mM L-glutamine (Sigma). For experimental analyses cells were seeded at 20–30% confluence on poly-D-lysine-coated (10 μg/ml in PBS) optic 96-well μ-clear plates (Greiner). 24 h later cells were transfected using jetPEI (PeqLab). For calcium imaging experiments receptors were cotransfected in equal amounts with the G protein subunit $G\alpha_{16}$. The best results were obtained in HEK293T PEAKrapid cells (ATCC).

Immunocytochemistry—Cells were fixed for 4 min in 4% methanol-free paraformaldehyde (Polyscience, Inc.) and permeabilized with 0.3% Triton X-100 for 4 min (for cell surface expression this step was omitted). After blocking with 5% FCS in PBS for 30 min cells were incubated overnight with an anti-rhodopsin monoclonal mouse IgG (1/500) of either anti-B6-30 (Dr. W. Clay Smith, University of Florida, Gainesville) or anti-4D2 (Dr. R. Molday, Centre for Macular Research, University of British Columbia, Canada). Staining was obtained by a 45-min incubation with a polyclonal goat anti-mouse Alexa Fluor 488 antibody (Invitrogen) at a 1/500 dilution. The total cell number was obtained by a counterstaining of the cell nuclei with Hoechst 33342 (Hoechst) 1/10,000. All solutions were diluted in PBS + 5% FCS. Receptor expression was analyzed 48 h after transfection. Pictures were taken using the imaging system BD Pathway Bioimager 855 (BD Biosci-

ences) and quantified with BD-image Explorer software (BD Biosciences).

Calcium Imaging and Data Analysis—High throughput measurements of population responses were performed using a fluorescence imaging plate reader (FLIPR) system (Molecular Devices) essentially as described previously (31). On average, a single well contained ~50,000 cells in these experiments. Briefly, 48 h after transfection cells were incubated with 2 μM
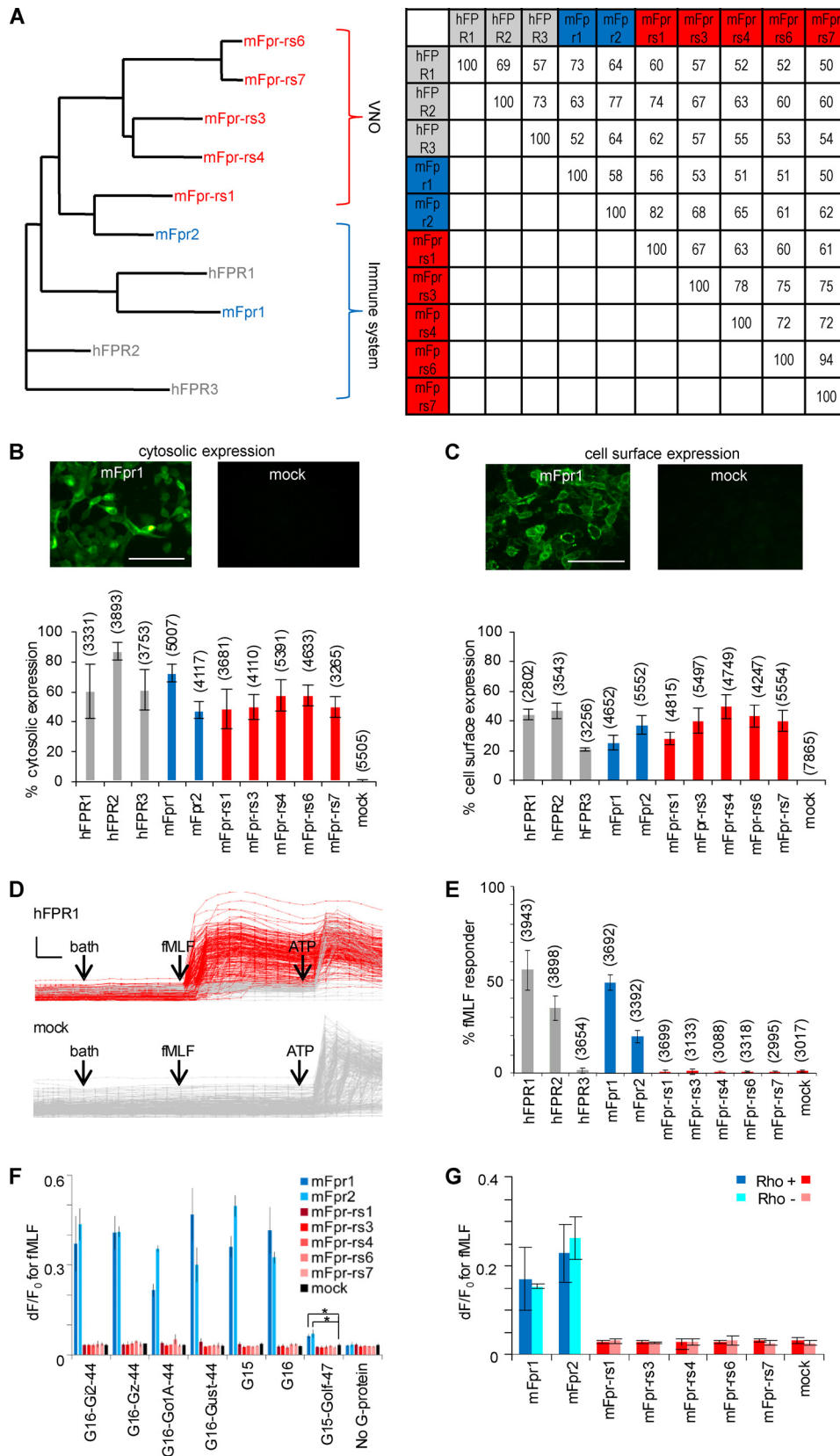
Fluo-4 AM (Molecular Probes) and 50 μM probenicid (Sigma) for 2 h at room temperature in a C1 bath solution (130 mM NaCl, 10 mM HEPES, 5 mM KCl, 2 mM CaCl$_2$, 5 mM glucose, pH 7.2). Before each experiment cells were rinsed three times with C1. Response amplitudes ($\Delta F/F_0$) were calculated by dividing the maximal change in fluorescence after ligand application by base-line fluorescence. Dose-response curves were calculated with GraphPad Prism 3.0 using the equation for sigmoidal dose response with variable slope. Statistical significance was analyzed in Excel using unpaired, two-tailed t tests. All experiments with mouse Fprs were performed in duplicate wells using at least three independent transfections.

For automated high throughput Ca^{2+} imaging with single-cell resolution, we used the BD Pathway Bioimager 855 system. Cells were loaded with Fura-2/AM using the Ratiomax Calcium Assay kit (BD Biosciences). Transfected cells were labeled by cotransfecting a plasmid encoding enhanced GFP in a dilution of 1/10 in addition to a given receptor and Gα_{16}. Calcium-dependent fluorescence signals of enhanced GFP-positive cells were recorded at 0.5 Hz. 30 μM ATP served as a positive control to monitor excitability of the cells. Cells that responded to buffer C1 were excluded from analysis. Images were taken with the Bioimager 855 system and quantified using Attovision software (BD Biosciences).

Ligands—The purity of all ligands was >95%. CRAMP33, CRAMP39, and rCRAMP33 were obtained from Innovagen. Temporin A amide, T20, ADP715 HIV-I, V3gp120 HIV (JR-FL), V3gp120 HIV (BK-130), μPAR 84-95, and β-amyloid$_{16-22}$ were purchased from Annaspec/MoBiTec. fMLF and DMSO were obtained from Sigma. Lipoxin A4 and 15-(R)-epi-lipoxin were obtained from Cayman Chemical. Ac2-26 and W-peptide were purchased from Tocris and Innovagen, respectively. COI-3I, NDI-6I, and all W-peptide derivatives were synthesized by GenScript Corporation. Initially, we dissolved all hydrophobic ligands in DMSO until we found that DMSO, at high concentrations, activates immune Fprs. Subsequently, all ligands were routinely dissolved in bath solution C1, except for lipoxin A4 and 15-(R)-epi-lipoxin, which were dissolved in ethanol. Under these conditions, most ligands tested in this study showed clear activation of immune Fprs. This result demonstrates the effectiveness of these ligands even when dissolved in aqueous solution. However, we cannot fully rule out moderate differences in the extent of solubility in C1 buffer *versus* a mixture of C1 and DMSO. The peptides ADP715 HIV-I and μPAR 84-95 did not activate any Fprs whereas V3gp120 HIV (JR-FL) only weakly activated hFPR3. To exclude that this could be due to solubility problems, we tested these compounds on all Fprs after dissolving them in DMSO but obtained virtually the same results (data not shown).

RESULTS

Heterologous Expression of Fprs from Immune and Vomeronasal Systems—To investigate the functional properties of Fprs, we established a heterologous expression system that enabled us to measure agonist-induced, receptor-dependent Ca^{2+} elevations in individual cells or cell populations. Adequate expression and correct cell surface localization of receptors is critical for their functional characterization in heterologous test systems. Although immune and vomeronasal Fprs are structurally related (Fig. 1A), their differences could influence expression in HEK293T cells. We first examined expression levels of all known human and mouse Fprs using immunocytochemistry. Thus far, most members of the murine Fpr family lack well characterized antibodies. To overcome this limitation, we fused the N terminus of the receptors with an epitope containing the first 39 amino acids of bovine rhodopsin and examined the cytosolic expression levels of these fusion proteins with an antibody directed against this Rho-epitope (32). We observed a high rate of receptor expression, ranging from 47 to 87% of the cells with a mean value of 60% $\pm$ 10% (Fig. 1B). Because the tag was localized at the extracellular side of the plasma membrane, we could monitor for all receptors whether they reach the cell surface. The percentage of cells with a detectable cell surface expression rate ranged from 21 to 46%, with a mean of 37 $\pm$ 6% (Fig. 1C). Hence, expression and localization of these receptors in HEK293T cells are highly appropriate for functional studies.

Next, we used single-cell resolution Ca^{2+} imaging to test whether receptor activation can be detected (Fig. 1, D and E). In this first experiment, we stimulated all family members with the prototypical ligand fMLF (9 μM). Consistent with previous observations (30, 33, 34), we found that cells expressing mFpr1 or mFpr2 and their human counterparts hFPR1 and hFPR2 could be activated by fMLF, whereas all other family members did not respond. In line with our expectations, the

FIGURE 1. **Immune and vomeronasal Fprs can be functionally expressed in HEK293T cells.** *A*, phylogenetic relationship (*left*) and sequence similarity in percentage (*right*) between mouse vomeronasal Fprs (*red*) and human (*gray*) and mouse (*blue*) immune Fprs. The human *FPR* family comprises three intact genes (*hFPR1*, *hFPR2*, and *hFPR3*) that are all expressed in immune cells. In rodents, the *Fpr* gene family underwent species-specific expansion containing seven intact *Fprs* in mice (44), which can be separated in two distinct sequence-related groups (18): one contains immune system Fprs expressed in leukocytes; the other vomeronasal Fprs that are predominantly or exclusively expressed in VSNs. The phylogenetic tree and similarity table were generated with Vector NTI 9.0. *B*, *upper*, representative immunostaining of permeabilized cells using an antibody directed against Rho tag to visualize total receptor expression. Cells were either transfected with mFpr1 or empty vector. *Scale bar*, 40 μm. *Lower*, quantification of cytosolic receptor expression. *Numbers* in *parentheses* above each *bar* denote the number of analyzed cells. *Error bars*, S.D. *C*, *upper*, Rho tag immunostaining of nonpermeabilized cells to visualize exclusively receptor expression at the cell surface (mFpr1 or empty vector expression). *Scale bar*, 40 μm. *Lower*, quantification of receptor cell surface expression. *D*, calcium transients upon agonist stimulation. Each *trace* represents a separate cell. *Upper*, traces of 364 cells transfected with hFPR1 of which 258 cells (*red*) responded to 9 μM fMLF. *Lower*, 337 mock-transfected cells served as negative control. Application of C1 buffer was used as a control to exclude any mechanical activation; 30 μM ATP that activates endogenous receptors was used as control for cell viability. *E*, quantification of the single-cell Ca^{2+} responses to 9 μM fMLF. *Scale*: $A_{340/380}$ ratio, 1; *time*, 0.5 min. *F*, effects of a range of G proteins on Fpr-mediated mean Ca^{2+} responses. Cell populations were cotransfected with a chimeric G protein and a given receptor in a 1:1 ratio. Ca^{2+} peak amplitudes after stimulation with 33.3 μM fMLF were plotted. *Mock*, cotransfection of the G protein together with an empty expression vector that was used to subclone the Fprs. *, $p \leq 0.05$. G proteins used were G$_{15}$, G$_{16}$, and corresponding G protein chimeras in which the last 44–47 amino acids were replaced by that of G$_{i2}$, G$_{z}$, G$_{o1A}$, G$_{olf}$, or G$_{gustducin}$. *G*, to rule out any effects of the Rho tag on receptor function, we compared mean Ca^{2+} peak responses with 9 μM fMLF (*chart bars* are mean values of nine wells from three independent FLIPR experiments) in cell populations that were transfected either with Rho-tagged receptors or unmodified receptors.

number of responding cells correlated well with the percentage of cells that express the receptors at the cell surface (Fig. 1, *C* and *E*).

To ensure efficient coupling of Fprs to downstream Ca^{2+} signaling pathways, we cotransfected the cells with the G_q-type G protein subunit $G\alpha_{16}$. This subunit is highly promiscuous and known to couple a wide variety of G protein-coupled receptors to $InsP_3/Ca^{2+}$ pathways that normally interact with $G\alpha_s$ or $G\alpha_i$-type G proteins (35). Under these conditions, we observed robust responses of human and mouse immune Fprs to the classical agonist fMLF; however, none of the vomeronasal Fprs responded (Fig. 1E). We examined whether the lack of response of vomeronasal Fprs could reflect a failure to interact with $G\alpha_{16}$. For instance, it is well known that the interaction between $G\alpha_{16}$ and receptors that couple via G_i, G_s, or G_o can be improved by C-terminal modifications of $G\alpha_{16}$ (36). We, therefore, tested several G protein chimeras in which the last 44–47 C-terminal amino acids of $G\alpha_{16}$ were replaced by those of other G protein α-subunits including chimeras of G_{i2} and G_{o1A}, both of which are expressed in mouse VSNs (Fig. 1F). We observed that immune Fprs are quite promiscuous and can interact with a variety of G protein chimeras containing C termini from G_o, G_q, G_i, and even G_s. However, compared with $G\alpha_{16}$, there was neither activation of vomeronasal Fprs nor strong enhancement of immune Fpr responses. Therefore, we employed the naturally occurring $G\alpha_{16}$ in all subsequent experiments.

To rule out that N-terminal modification affected subcellular distribution and receptor function, we assessed whether fusion of the receptors with the Rho-epitope altered their function. We compared mean Ca^{2+} responses of cell populations expressing either native or Rho-epitope-tagged receptors upon stimulation with fMLF but found no obvious functional differences (Fig. 1G). Nonetheless, we decided to use only unmodified receptors in subsequent functional studies to exclude any possible experimental bias.

Finally, to investigate whether our assay is equally suited to monitor receptor activation to other ligands, we tested the well characterized human receptors with a selection of other known agonists. We observed robust Ca^{2+} elevations to classical Fpr agonists including W-peptide, T20, Temporin A amide, Ac2-26, COI, NDI, and V3gp120 (Fig. 2). Together, these findings demonstrate the validity of our assay for the functional characterization of members of the Fpr family.

Ligand Selection—We next tested cells transfected with a given Fpr using a panel of 32 selected compounds that cover several known ligand classes of the human Fpr family (Figs. 3 and 4). Our ligand selection included 16 naturally occurring substances comprising two immunomodulatory eicosanoids and 14 formylated and nonformylated bacterial, viral, antimicrobial, or endogenous immunomodulatory peptides. Initial experiments revealed that three of four tested antimicrobial peptides (CRAMP33, CRAMP39, rCRAMP33) elicited large, unspecific Ca^{2+} signals that were receptor-independent because these signals also occurred in mock-transfected cells (Fig. 3, *B* and *C*). Therefore, these compounds were excluded from further investigations. We also tested 13 novel synthetic peptides that proved to be important for the analysis of mFprs1 (see below and Fig. 4).
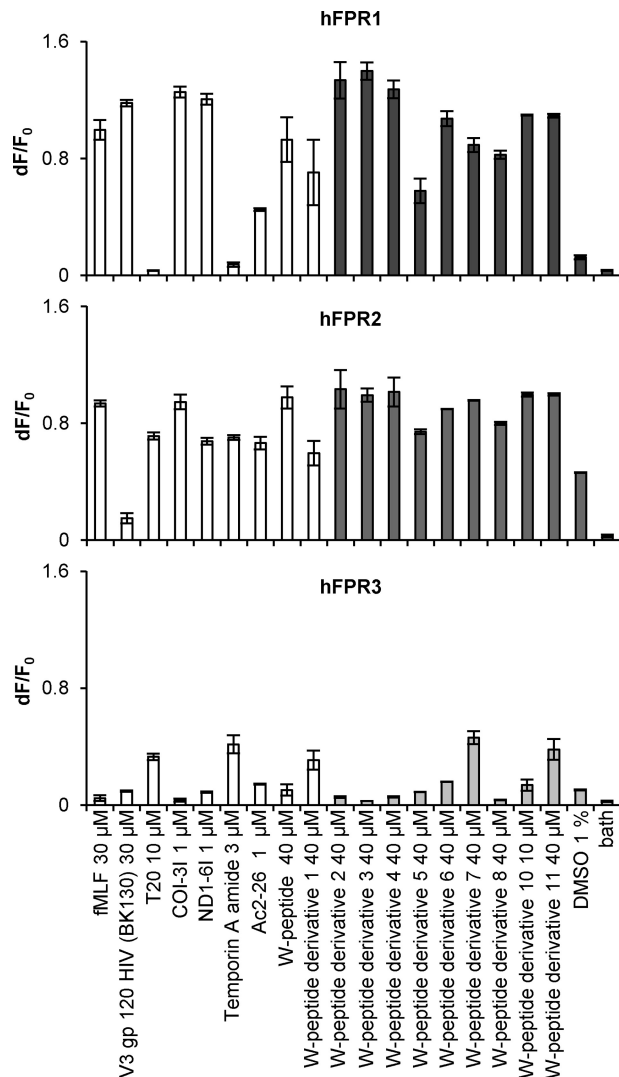
FIGURE 2. **Analysis of Ca^{2+} responses of three human FPRs to selected ligands.** *Bars* display peak amplitudes of Ca^{2+} elevations to ligand stimulation as mean increase over base-line fluorescence. *White bars* denote responses to prototypical hFPR agonists, and *gray bars* indicate responses to novel W-peptide derivatives. *Error bars*, S.D.

Unexpectedly, we observed in initial experiments that the organic solvent DMSO activates cells expressing mFpr1 or mFpr2 at certain concentrations but not cells that expressed other members of the mouse Fpr receptor family (Figs. 3A and 5B). The observed threshold of activation for both receptors was ~0.1%, and saturation was reached at ~3%. DMSO activation of both receptors showed clear dose-dependence, with an EC_{50} of 97 mM for mFpr1 and an EC_{50} of 111 mM for mFpr2 (Fig. 5B). Unspecific DMSO-dependent signals in the mock-transfected negative controls could only be seen at concentrations >2% and showed different kinetics (Fig. 5B). DMSO-evoked signals depended on the presence of $G\alpha_{16}$ (Fig. 5C) and the mFpr receptor (Fig. 5D). Notably, the human receptor hFPR2 was also susceptible to 1% DMSO (Fig. 2). Thus, our results show that the use of DMSO as an organic solvent is critical, and concentrations >0.1% should be avoided in functional studies of mouse or human Fprs. To exclude any possible experimental bias, we decided to dissolve all agonists directly in the assay buffer C1.
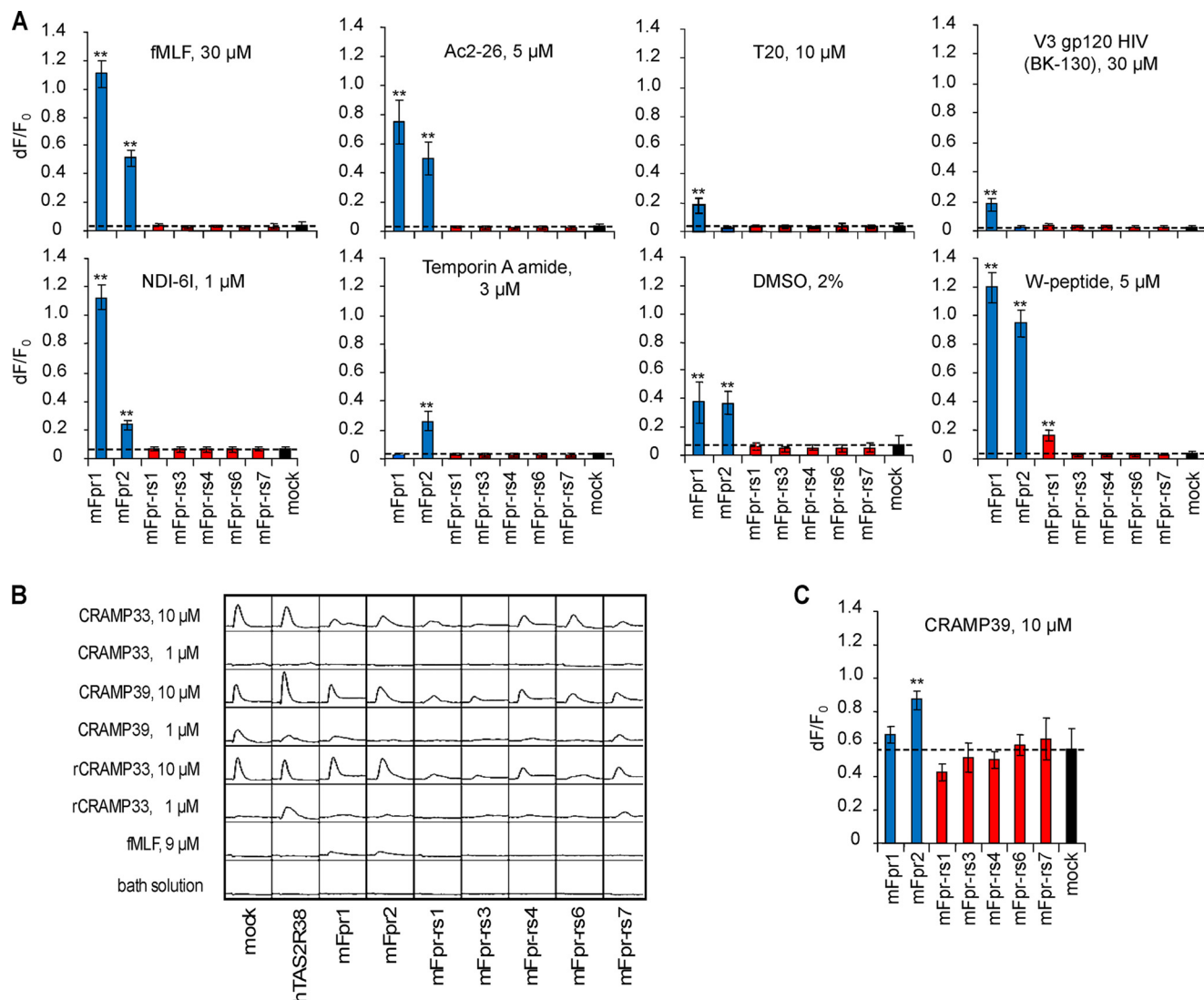
FIGURE 3. **Mouse and human immune Fprs exhibit similar agonist profiles whereas vomeronasal Fprs are functionally distinct.** *A*, mean Ca^{2+} peak responses of all mouse Fpr receptors to selected ligands. Each *bar* is based on triplicate measurements from at least three independent transfections. **, $p \leq$ 0.01. *B*, representative Ca^{2+} waveforms from FLIPR experiments to CRAMP application. CRAMP elicits robust but unspecific Ca^{2+} signals. Typical Ca^{2+} traces of a FLIPR experiment upon stimulation with two different CRAMP concentrations are shown. The observed signals do not depend on Fpr expression because they can also be observed in mock-transfected cells and in cells transfected with the bitter taste receptor hTAS2R38, both of which serve as negative controls. Similar concentrations of the well established Fpr agonist fMLF only activated cells transfected with mFpr1 and mFpr2. *C*, mean Ca^{2+} peak responses of all mouse Fpr receptors to 10 μM CRAMP39. *Bars* denote mean responses of triplicates over three independent transfections. *Error bars*, S.D. **, $p \leq 0.01$ compared with mock control.

Agonist Profiles of Mouse and Human Immune Fprs Match Closely—By testing our ligand collection on all mouse and human Fprs, we observed a surprisingly high degree of overlap in agonist profiles between the human receptors hFPR1 and hFPR2 and their murine counterparts mFpr1 and mFpr2 (Fig. 4). These receptors showed very similar response profiles to 25 of 29 compounds. Three of the remaining compounds could at least activate a single receptor in both species. Importantly, β-amyloid$_{16-22}$ was the only molecule that exhibited a clear species-specific activation pattern because it robustly activated mouse Fpr1 but none of the human receptors (Fig. 4). Moreover, comparison of W-peptide concentration-response curves demonstrated a remarkable functional conservation between immune system-derived human FPRs and their murine counterparts. The EC$_{50}$ values of hFPR1 and hFPR2 were 5 nM and 1 nM, respectively, closely similar to those of mFpr1 and mFpr2 (3

nM and 5 nM, respectively) (Fig. 6B). Thus, despite ~100 million years of divergent evolution, the EC$_{50}$ profiles for this compound are still nearly identical.

Identification of Subtype-selective Agonists for Mouse Immune Fprs—We also observed a considerable, functional similarity between mFpr1 and mFpr2: 21 compounds were capable of stimulating both mouse receptors (Fig. 4). Despite this overlap in ligand profile, we identified several subtype-selective agonists (Fig. 5A). Temporin A amide was a selective agonist of mFpr2 at all tested concentrations (EC$_{50}$ 0.7 μM). T20 and β-amyloid$_{16-22}$ were selective for mFpr1, with an EC$_{50}$ of 0.2 μM and 4 μM, respectively. V3gp120 HIV (BK-130) and NDI-6I were strongly preferential activators of mFpr1. The sensitivity of mFpr1 for NDI-6I was ~100-fold higher than that of mFpr2: NDI-6I activated mFpr1 with an EC$_{50}$ of 0.6 nM compared with 57 nM for mFpr2. The activation threshold of

ligand	primary structure	ligand class	Highest tested concentration	hFPR1	hFPR2	hFPR3	mFpr1	mFpr2	mFpr-rs1	mFpr-rs3	mFpr-rs4	mFpr-rs6	mFpr-rs7
fMLF	f-MLF	bacterial peptide	30 μM	●	●	○	●	●	○	○	○	○	○
ADP715, HIV-I	RKRIHIGPGRAFYTTKN	viral peptide	30 μM	○	○	○	○	○	○	○	○	○	○
V3 gp120 HIV (JR-FL)	SIHIGPGRAFYTT	viral peptide	30 μM	○	○	(●)	○	○	○	○	○	○	○
V3 gp120 HIV (BK-130)	RIHIGPGRALYTT	viral peptide	30 μM	●	(●)	(●)	●	(●)	○	○	○	○	○
T20	Ac-YTSLIHSLIEESQNQQEKNEQELLELDKWASLWNWF-(NH2)	viral peptide	10 μM	○	●	●	●	○	○	○	○	○	○
COI-3I	f-MFINRWLFS	mitochondrial peptide	1 μM	●	●	●	●	●	○	○	○	○	○
NDI-6I	f-MFFINILTL	mitochondrial peptide	1 μM	●	●	○	●	●	○	○	○	○	○
CRAMP33	GLLRKGGEKIGEKLKKIGQKIKNFFQKLVPQPEQ	anti microbial peptide	10 μM	u.s.	u.s.	u.s.	u.s.	u.s.	u.s.	u.s.	u.s.	u.s.	u.s.
CRAMP39	ISRLAGLLRKGGEKIGEKLKKIGQKIKNFFQKLVPQPEQ	anti microbial peptide	10 μM	u.s.	u.s.	u.s.	u.s.	u.s.	u.s.	u.s.	u.s.	u.s.	u.s.
rCRAMP33	GLLRKGGEKFGEKLRKIGQKIKDFFQKLAPEIEQ	anti microbial peptide	10 μM	u.s.	u.s.	u.s.	u.s.	u.s.	u.s.	u.s.	u.s.	u.s.	u.s.
Temporin A amide	FLPLIGRVLSGIL-(NH2)	anti microbial peptide	3 μM	○	●	●	○	●	○	○	○	○	○
Lipoxin A4	$C_{20}H_{32}O_5$	immunomodulatory eicosanoid	1 μM	○	○	○	○	○	○	○	○	○	○
15-(R)-Epi-Lipoxin	$C_{20}H_{32}O_5$	immunomodulatory eicosanoid	1 μM	○	○	○	○	○	○	○	○	○	○
beta-amyloid 16-22	KLVFFAE	immunomodulatory peptide	10 μM	○	○	○	●	○	○	○	○	○	○
Ac2-26	Ac-AMVSEFLKQAWFIENEEQEYVQTVK	immunomodulatory peptide	5 μM	●	●	●	●	●	○	○	○	○	○
uPAR 84-95	Ac-AVTYSRSRYLEC-(NH2)	immunomodulatory peptide	10 μM	○	○	○	○	○	○	○	○	○	○
DMSO	C_2H_6OS	organic solvent	5.6×10^5 μM	○	●	○	●	●	○	○	○	○	○
W-peptide	WKYMVm-(NH2)	synthetic peptide	30 μM	●	●	(●)	●	●	●	○	○	○	○
W-peptide derivative 1	WKYMVM-(NH2)	synthetic peptide	40 μM	●	●	(●)	●	●	(●)	○	○	○	○
W-peptide derivative 2	KYMVm-(NH2)	synthetic peptide	40 μM	●	●	○	●	●	●	○	○	○	○
W-peptide derivative 3	YMVm-(NH2)	synthetic peptide	40 μM	●	●	○	●	●	●	○	○	○	○
W-peptide derivative 4	MVm-(NH2)	synthetic peptide	40 μM	●	●	○	●	●	○	○	○	○	○
W-peptide derivative 5	Vm-(NH2)	synthetic peptide	40 μM	●	●	○	●	●	○	○	○	○	○
W-peptide derivative 6	WKYMVVm-(NH2)	synthetic peptide	40 μM	●	●	(●)	●	●	●	○	○	○	○
W-peptide derivative 7	WKYMVmm-(NH2)	synthetic peptide	40 μM	●	●	●	●	●	○	○	○	○	○
W-peptide derivative 8	WKYMVm	synthetic peptide	40 μM	●	●	○	●	●	(●)	○	○	○	○
W-peptide derivative 9	AWKYMVm-(NH2)	synthetic peptide	40 μM	●	●	●	●	●	●	○	○	○	○
W-peptide derivative 10	WKYMVc-(NH2)	synthetic peptide	40 μM	●	●	(●)	●	●	●	○	○	○	○
W-peptide derivative 11	WKYMVC-(NH2)	synthetic peptide	40 μM	●	●	●	●	●	○	○	○	○	○
W-peptide derivative 12	Ac-WKYMVm-(NH2)	synthetic peptide	30 μM	●	●	n.d.	●	●	●	○	○	○	○
W-peptide derivative 13	AAWKYMVm-(NH2)	synthetic peptide	30 μM	●	●	n.d.	●	●	●	○	○	○	○
W-peptide derivative 14	f-AWKYMVm-(NH2)	synthetic peptide	30 μM	●	●	●	●	●	●	○	○	○	○

FIGURE 4. **Mouse and human immune Fprs are functionally conserved, whereas the agonist profile of vomeronasal Fprs shows little overlap.** Summary of response profiles of all tested receptors to the highest tested ligand concentration. Each result represents duplicate measurements from at least three independent transfections. ●, robust, receptor-dependent Ca^{2+} signal; (●), weak signal; ○, no response; *u.s.*, strong but unspecific response, observed in mock-transfected cells; *n.d.*, not determined. Peptide sequences are shown in one-letter amino acid code. *Underlined letters* represent chemical modifications: *Ac*, acetylated N terminus; *c*, D-cysteine; *m*, D-methionine; *f*, formylated N terminus; *NH₂*, amidated C terminus.

V3gp120 HIV (BK-130) for mFpr1 was ∼1 μM and its EC_{50} was 4.5 μM. We could only see a weak activation of mFpr2 at concentrations of ≥30 μM. Interestingly V3gp120 HIV (JR-FL), which has a high degree of sequence similarity to V3gp120 HIV (BK-130), did not activate any of the mouse receptors. Instead, it was a selective activator of human hFPR3.

Selective Tuning of Vomeronasal mFpr-rs1 versus Immune Fprs—Compared with the remarkable functional similarity and the broadly tuned agonist profiles of mouse and human immune Fprs, we observed relatively narrow tuning for the vomeronasal receptor mFpr-rs1. This receptor responded to W-peptide, a synthetic ligand for mFpr1, mFpr2, and all human Fprs (37) (Fig. 6, *A* and *B*). Despite robust activation of mFpr-rs1 by W-peptide and several chemically related derivatives (Fig. 6, *C–F*), we did not detect activation of this receptor by any of the other tested Fpr ligands (Fig. 4). The immune receptors mFpr1 and mFpr2 were at least ∼200-fold more sensitive to W-peptide than mFpr-rs1 (Fig. 6B). Structural W-peptide
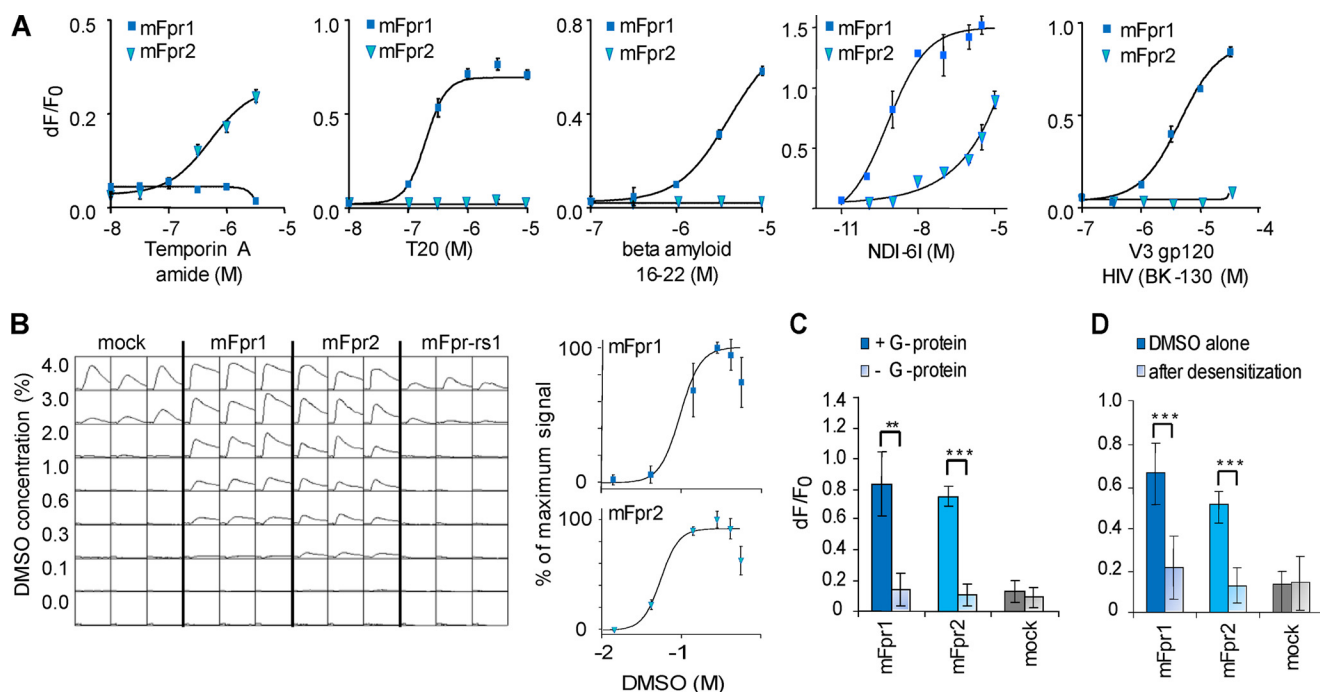
FIGURE 5. **Concentration-response curves of two mouse immune Fprs (mFpr1 and mFpr2) for selected agonists.** *A*, our analysis revealed several subtype-specific agonists. Temporin A amide is selective for mFpr2 and has an EC_{50} of 690 nM. T20, β-amyloid$_{16-22}$ and V3gp120 HIV (BK-130) are selective for mFpr1 with an EC_{50} of 200 nM, 4,100 nM, and 4,500 nM, respectively. NDI-6I prefers mFpr1 with an EC_{50} of 0.6 nM but can also activate mFpr2 with an EC_{50} of 57 nM. *B*, mFpr1 and mFpr2 but not mFpr-rs1 are activated by DMSO at concentrations above 0.1%. First unspecific effects of DMSO are observed above 2%. The DMSO activation is dose-dependent with an EC_{50} of 97 mM for mFpr1 and 111 mM for mFpr2. These experiments are based on at least five independent transfections. *C*, analysis of Ca^{2+} signals evoked by DMSO (2%). These signals depend on the presence of the G protein α-subunit $G\alpha_{16}$. *Bars* show mean responses of duplicates for two independent transfections. *D*, cross-desensitization of DMSO (2%) evoked Ca^{2+} responses by fMLF (30 μM). *Bars* show mean responses of triplicates for three independent transfections. *Error bars*, S.D. **, $p \leq 0.01$; ***, $p \leq 0.001$.

derivatives that activated mFpr-rs1 were also capable of activating mFpr1 and mFpr2. Together, these findings provide clear evidence that the agonist profile of mFpr-rs1 is distinct from that of mFpr1 and mFpr2. This conclusion extends also to the remaining four vomeronasal Fprs because these did not respond to any of the tested compounds under the conditions used here (Fig. 4).
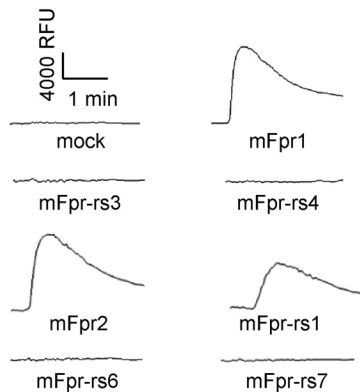
mFpr-rs1 Shows Stereo-selective Tuning for Related Peptides Containing D-Amino Acids—To identify key structures in W-peptide that are necessary for the activation of mFpr-rs1, we designed and tested a small library of 14 derivatives (Fig. 6, *C–F*). W-peptide, a hexapeptide, shows a remarkable structural feature because it contains an amidated D-methionine at its C terminus. Although enzymatic amidation of peptides is frequently observed, the occurrence of D-amino acids in nature is relatively rare. Most natural proteins and peptides consist of L-amino acids. However, certain pathogens provide a potent natural source for D-amino acids because these amino acids exist in the cell wall of bacteria or in toxins secreted by fungi. Therefore, we tested the stereo-selectivity of mFpr-rs1 by using the L-isomer of W-peptide (Fig. 6C). We observed a ~25-fold rightward shift in EC_{50} value of L-W-peptide, indicating that the receptor shows a clear preference for the D-form. Furthermore, maximum amplitude for L-W-peptide was reduced by 69 ± 9%, suggesting that this compound acts as a partial agonist of mFpr-rs1 (Fig. 6C). Next, we tested whether D-methionine can be substituted by D-cysteine. Again, we observed clear activation demonstrating that the receptor also responds to peptides containing this D-amino acid (Fig. 6C). However, such

peptides are less preferred by the receptor because we observed a ~40-fold rightward shift in EC_{50} values. Substitution of D-cysteine by the corresponding L-form caused a 10-fold increase in activation threshold (Fig. 6C). On the basis of these findings, we conclude that mFpr-rs1 prefers D-amino acid-containing peptides.
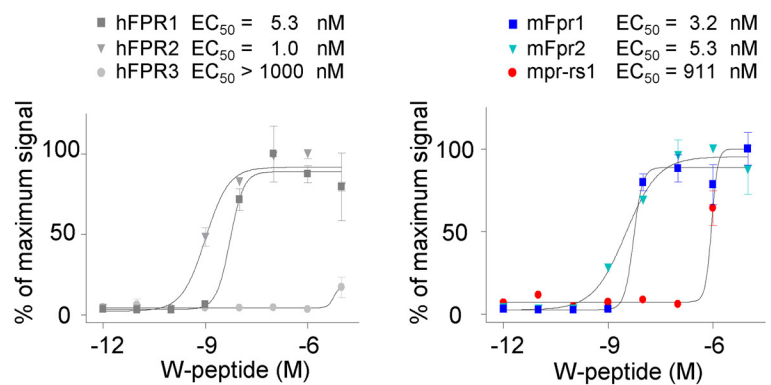
We also determined the influence of N-terminal amino acids on mFpr-rs1 activation (Fig. 6, *D* and *E*). Interestingly, mFpr-rs1 seems to tolerate N-terminal elongations because such manipulation, by addition of one or two alanine residues, did not alter its sensitivity (Fig. 6E). Insertion of a valine directly in front of the D-methionine led to a drastic ~30-fold rightward shift of the EC_{50} value (Fig. 6E). Addition of a second D-methionine at its C terminus caused a complete loss of the capability to activate mFpr-rs1, whereas mFpr1 and mFpr2 could still be activated (Figs. 6E and 4). This demonstrates the importance of the C terminus for mFpr-rs1 activation although a considerable amount of flexibility in N-terminal length is permitted. Deletion of the first N-terminal amino acid positions had only a moderate influence on the receptor response (Fig. 6D). By contrast, a ~70-fold lower sensitivity was observed when the first two amino acids were removed (Fig. 6D). The deletion of the first three amino acids that included the tyrosine in the third position resulted in a complete loss of the capability to activate mFpr-rs1 (Fig. 6D). However, the peptide could still interact with mFpr1 and mFpr2 (Fig. 4). Thus, tyrosine at amino acid position three is a key feature for interaction between W-peptide and mFpr-rs1 but is not required for mFpr1 and mFpr2. We also determined the influence of chemical modifications at

A, Calcium traces upon stimulation with W-peptide

B, Concentration response of mouse and human FPRs to W-peptide

■ hFPR1 EC_{50} = 5.3 nM
▼ hFPR2 EC_{50} = 1.0 nM
● hFPR3 EC_{50} > 1000 nM

■ mFpr1 EC_{50} = 3.2 nM
▼ mFpr2 EC_{50} = 5.3 nM
● mpr-rs1 EC_{50} = 911 nM

C, mFpr-rs1 response to peptides with C-terminal D- and L-amino acids

WKYMVm-(NH₂)
EC_{50} = 0.6 ±0.3 µM

WKYMV**M**-(NH₂)
EC_{50} = 15.5 ±3.5 µM

WKYMV**c**-(NH₂)
EC_{50} = 26.2 ±7.0 µM

WKYMV**C**-(NH₂)
EC_{50} > 100µM
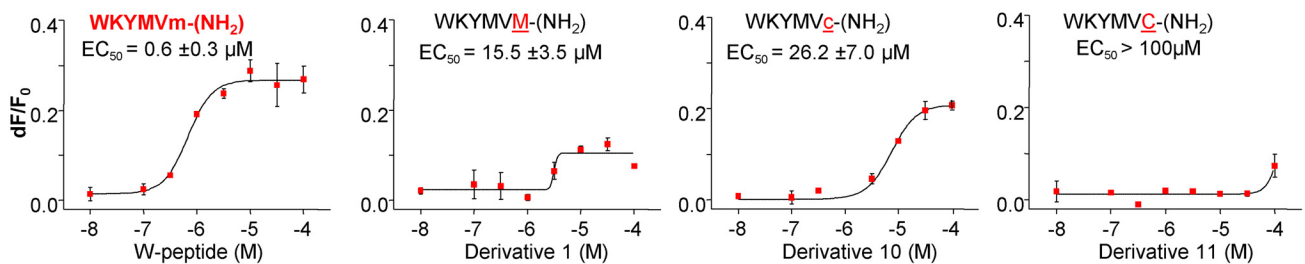
D, mFpr-rs1 response to peptides with shorter chain length

-KYMVm-(NH₂)
EC_{50} = 5.3 ±0.6 µM

--YMVm-(NH₂)
EC_{50} = 40.4 ±19.3 µM

---MVm-(NH₂)

----Vm-(NH₂)
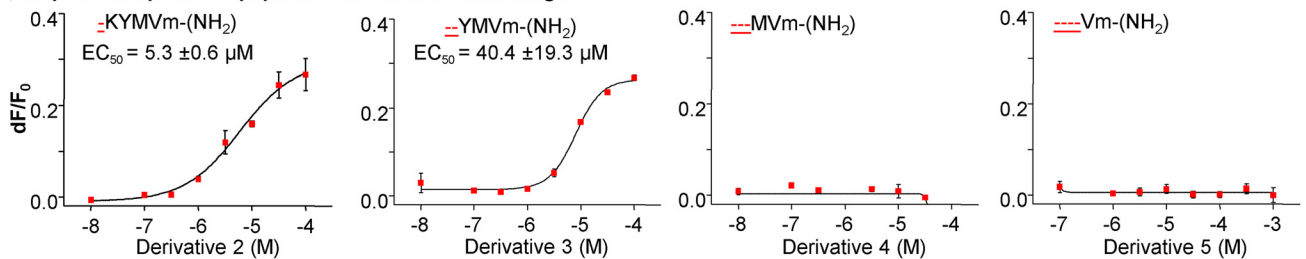
E, mFpr-rs1 response to peptides with longer chain length

AAWKYMVm-(NH₂)
EC_{50} = 0.4 ±0.1 µM

AWKYMVm-(NH₂)
EC_{50} = 0.5 ±0.3 µM

WKYMV**m**m-(NH₂)

WKYMV**V**m-(NH₂)
EC_{50} = 22.6 ±8.3 µM
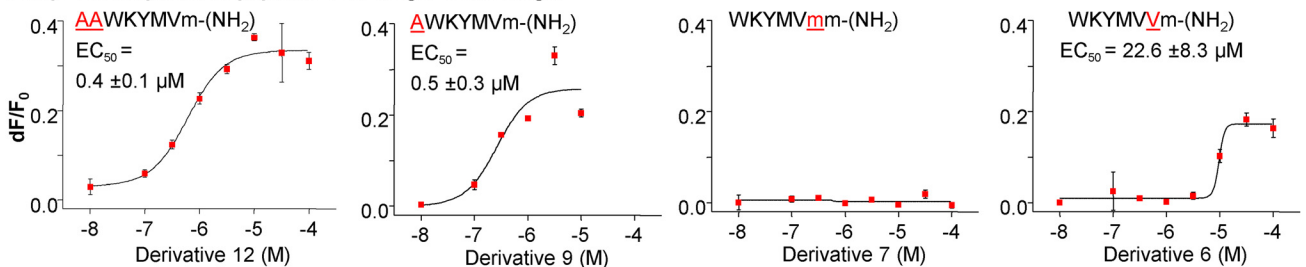
F, Influence of amidation, formylation and aectylation on the mFpr-rs1 response

WKYMVm-
EC_{50} = 23.4 ±5.0 µM

f-AWKYMVm-(NH₂)
EC_{50} = 1.8 ±1.5 µM

Ac-WKYMVm-(NH₂)
EC_{50} = 0.9 ±0.4 µM

A

(Ac) - N - N - W - K - **Y** - M - V - **m** - (NH$_2$)

■ strong effects on sensitivity
■ modulates sensitivity
■ weak effects

B

Motif	Total hits	bacteria	fungi	virus	mouse	human
WKYMVM	1	100%	0	0	0	0
KYMVM	367	76 %	10%	0.3%	0	0
YMVM	8160	58%	8%	0.5%	0.6%	1.3%

C

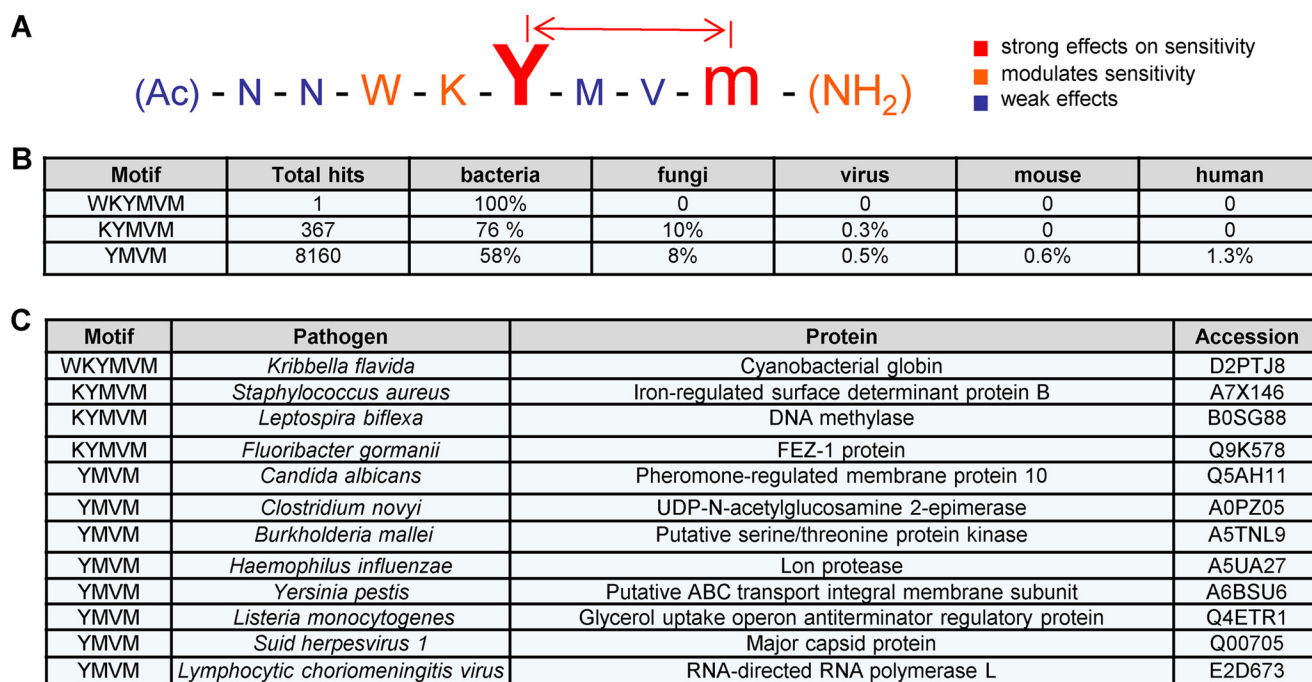| Motif	Pathogen	Protein	Accession
WKYMVM	*Kribbella flavida*	Cyanobacterial globin	D2PTJ8
KYMVM	*Staphylococcus aureus*	Iron-regulated surface determinant protein B	A7X146
KYMVM	*Leptospira biflexa*	DNA methylase	B0SG88
KYMVM	*Fluoribacter gormanii*	FEZ-1 protein	Q9K578
YMVM	*Candida albicans*	Pheromone-regulated membrane protein 10	Q5AH11
YMVM	*Clostridium novyi*	UDP-N-acetylglucosamine 2-epimerase	A0PZ05
YMVM	*Burkholderia mallei*	Putative serine/threonine protein kinase	A5TNL9
YMVM	*Haemophilus influenzae*	Lon protease	A5UA27
YMVM	*Yersinia pestis*	Putative ABC transport integral membrane subunit	A6BSU6
YMVM	*Listeria monocytogenes*	Glycerol uptake operon antiterminator regulatory protein	Q4ETR1
YMVM	*Suid herpesvirus 1*	Major capsid protein	Q00705
YMVM	*Lymphocytic choriomeningitis virus*	RNA-directed RNA polymerase L	E2D673

FIGURE 7. *A*, model indicating residues that are important for the interaction of W-peptide with mFpr-rs1. *B*, mFpr-rs1 agonist motifs frequently found in proteins of various microorganisms. *C*, natural pathogens that exhibit peptide agonist motifs for mFpr-rs1. These sequences were identified by a sequence scan in UniProtKB/Swiss-Prot, UniProtKB/TrEMBL from July 2012 using the ScanProsite software (release 20.83) and the taxa analysis tool.

the N and C termini (Fig. 6*F*). To investigate whether amidation of D-methionine affects its interaction with mFpr-rs1, we tested a structural homologue lacking C-terminal amidation. This procedure caused a clear 30-fold rightward shift (Fig. 6*F*). In contrast, N-terminal acetylation or formylation had no obvious effects on mFpr-rs1 activation (Fig. 6*F*). Thus, the last four C-terminal amino acids are critical for receptor-ligand interaction, whereas N-terminal modifications do not strongly alter receptor sensitivity. Hence, mFpr-rs1 could recognize a considerable number of structurally related proteins that show some common hallmarks (Fig. 7*A*). Importantly, such motifs occur in a wide variety of proteins that are preferentially found in natural pathogens (Fig. 7, *B* and *C*).

DISCUSSION

Several main findings emerge from the current work. We discovered several subtype-selective agonists for mouse immune Fprs and identified W-peptide and related structures as a new agonist class for the vomeronasal receptor mFpr-rs1. Using a novel chemical library, our experiments revealed stereo-selective tuning of mFpr-rs1 for related D-amino acid-containing peptides. Moreover, we identified specific motifs that are critical for mFpr-rs1 ligand-receptor interaction. Interestingly, such motifs exist in a variety of proteins derived from natural pathogens, supporting the proposed role of mFpr-rs1 in vomeronasal pathogen detection. Overall, our findings demonstrate that the agonist profile of mFpr-rs1 is distinct from that

of immune Fprs. Our results show widespread functional conservation between mouse and human immune Fprs and suggest a neofunctionalization of the vomeronasal Fprs.

Neofunctionalization of Mouse Formyl Peptide-related Receptors—Recent phylogenetic analysis of the Fpr family in mammals provided genetic evidence for a rodent-specific neofunctionalization of the vomeronasal Fprs in mouse (18). We here provide the first functional support for this hypothesis. In case of mFpr-rs1, we have clear evidence that its agonist spectrum is much more selective than that of mFpr1 and mFpr2. Despite robust activation of mFpr-rs1 by W-peptide and structural derivatives we did not observe any responses to other typical ligands that activate immune Fprs. Moreover, we showed that interaction of mFpr-rs1 with W-peptide is more restrictive in its structural requirements than that of mFpr1 or mFpr2 because several structural derivates that could not activate mFpr-rs1 still activated mFpr1 or mFpr2. We found that C-terminal amino acids of W-peptide are critical for ligand-receptor interaction, whereas changes in the N-terminal region are better tolerated (Fig. 7*A*).

Our ligand model predicts that a substantial number of chemically related peptides will activate mFpr-rs1. Moreover, there is the intriguing possibility that other peptide sequences or not yet tested posttranslational modifications may further enhance the receptor agonist interaction or enlarge the number of potential ligands. A particularly interesting feature of mFpr-

FIGURE 6. **Response of mFpr-rs1 to W-peptide derivates.** *A*, representative Ca^{2+} traces from FLIPR experiments of all mouse receptors to 5 μM W-peptide. *B*, comparison of concentration-response curves between mFpr-rs1 and the mouse and human immune Fprs. *C–F*, concentration-response curves of mFpr-rs1 to stimulation with structural derivatives of W-peptide. The lead structure of W-peptide is labeled in *red*. Modifications in the peptide structure are *underlined*. Peptide sequences are shown in one-letter amino acid code. L-Isomers are given in *capital letters* whereas D-isomers are displayed in *lowercase letters*. NH$_2$, amidated N terminus; *Ac*, acetylated N terminus; *f*, formylated N terminus. EC$_{50}$ values $\pm$ S.D. (*error bars*) represent mean values of duplicate measurements from at least three independent transfections.

rs1 is its strong stereo-selective preference for peptides with a D-amino acid in the last C-terminal position. This finding is rather surprising because D-amino acids are relatively rare in nature, and most natural proteins and peptides consist solely of L-amino acids (38). However, microorganisms are a potent natural source for D-amino acid-containing peptides, as these are found in the bacterial cell wall and in toxins secreted by fungi (38). Notably, a number of proteins in pathogens contain those peptide motifs that were identified in the present study (Figs. 6 and 7*B*). Thus, our ligand profile of mFpr-rs1 supports a role in vomeronasal pathogen detection although natural ligands still remain to be identified.

We did not detect any specific activation of the remaining four vomeronasal Fprs (mFpr-rs3, mFpr-rs4, mFpr-rs6, and mFpr-rs7) by our current ligand selection that focused on peptide agonists of immune Fprs. Responses to CRAMP33, CRAMP39, or rCRAMP33 also occurred in mock-transfected cells and, therefore, were nonspecific. A possible explanation is that vomeronasal Fprs may detect molecules that were lacking in our current ligand panel. Interestingly, mFpr-rs1 is expressed in the basal zone of the VNO epithelium (18, 19) which is known to detect peptide and protein cues (12). The remaining four vomeronasal Fprs are expressed in the apical zone of the VNO (18, 19) that responds predominantly to low molecular weight organic molecules (12). Thus, it is tempting to speculate that the Fprs in the apical zone may recognize ligands that are more similar to lipoxin A4, A14, or other small organic ligands rather than peptides. Alternatively, Fprs expressed in HEK cells could behave somewhat differently from those of native VSNs. For example, we have not yet determined the influence of known cofactors for immune Fprs, such as CD38 or MARCO (39, 40), that could modulate receptor responses. Differential expression of cofactors in HEK cells could be a potential factor to explain diverse results. We have no evidence for any alternative explanations such as difficulties in heterologous expression. Our immunohistochemical and functional results clearly show adequate expression and correct cell surface localization of all mouse Fprs. We also demonstrate that Fprs are quite promiscuous and readily interact with $G\alpha_{16}$ and several other G protein chimeras.

Functional Conservation between Human and Mouse Immune Fprs—We found substantial evidence for functional conservation between mouse mFpr1 and mFpr2 and their human counterparts hFPR1 and hFPR2. Remarkably, >90% of the tested compounds were detected by these receptors in both species. In case of W-peptide, even the concentration-response profiles were nearly identical. Given that both species split already ~100 million years ago (41) and the sequence identity between human and mouse Fpr1 and Fpr2 is only 73 and 77%, respectively, the extent of this functional conservation is surprisingly high. Thus, there may be similar biological constraints underlying the evolution of these receptors across both species. All four receptors are expressed in the immune system (21), and it seems that they have closely similar functional requirements in pathogen detection and immune function, despite the fact that both species vary strongly in their susceptibility to infections by different pathogenic strains. These findings support a model in which immune Fprs are highly sensitive, global che-

modetectors for a wide variety of components released by fungi, bacteria, and viruses or endogenous tissues during infections or inflammatory processes. By contrast, hFPR3, which is also expressed in human monocytes and mature dendritic cells, seems to have a more restricted biological function because many of the compounds that activated both hFPR1 and hFPR2 did not activate hFPR3. In line with previous results (20), we observed that the sensitivity of hFPR3 toward most activators was drastically lower than that of hFPR1 or hFPR2.

Agonist Properties of Mouse and Human Fprs—We observed that DMSO, which we initially used as an organic solvent, activates cells expressing hFPR2. This is of considerable interest because DMSO is used not only as a solvent but also as a drug in diverse therapeutic treatments (42). Our observation might, therefore, help to explain some of the well known immune modulatory effects of DMSO on human leukocytes (42). Furthermore, we discovered several novel agonists to examine the biological function of individual receptors: Temporin A amide as a selective agonist for mFpr2, and T20, β-amyloid$_{16-22}$, and V3gp120 HIV (BK-130) as selective activators of mFPR1. Interestingly, the structurally closely related V3gp120 HIV (JR-FL) is a selective activator of human hFPR3 but did not activate any of the mouse receptors. Hence, small sequence variations in these ligands can be sufficient to alter receptor activation strongly. Moreover, we observed that mFpr1 is ~100-fold more sensitive to the mitochondrial formyl peptide NDI-6I than mFpr2. With an EC_{50} in the picomolar range, NDI-6I is one of the most sensitive activators of mFpr1. Our results also show that T20 is a selective agonist of mFpr1. This fits well with previous findings indicating that T20 loses its chemotactic effects on neutrophils in mFpr1-deficient mice (43). However, Ref. 43 also reports an activation of mFpr1 and mFpr2 by T20 in HEK293 cells, which is inconsistent with the lack of response of leukocytes in mFpr1-deficient mice (43). Moreover, it was recently reported that CRAMP specifically activates all five mouse vomeronasal Fprs when expressed heterologously (19). We were unable to confirm specific activation by CRAMP because of high unspecific, endogenous background signals to this ligand (Fig. 3*B*). The same study also reported that fMLF activated four of the five vomeronasal Fprs. In line with other investigations (18, 29, 30, 43, 44) we did not observe any activation of a vomeronasal Fpr by fMLF. One future experimental strategy that may resolve these questions is combining results from *in vitro* studies with those of native VSNs expressing known Fprs. In pilot studies, we already observed that a small subfraction of VSNs exhibits stereo-selective tuning to D-W-peptide. However, given that V2R receptors also recognize short peptides (9), formal proof that these neurons indeed express mFpr-rs1 will be crucial.

REFERENCES

1. Kavaliers, M., Choleris, E., and Pfaff, D. W. (2005) Genes, odours and the recognition of parasitized individuals by rodents. *Trends Parasitol.* **21,** 423–429

2. Shirasu, M., and Touhara, K. (2011) The scent of disease: volatile organic compounds of the human body related to disease and disorder. *J. Biochem.* **150,** 257–266

3. Ferrero, D. M., and Liberles, S. D. (2010) The secret codes of mammalian scents. *Wiley Interdiscip. Rev. Syst. Biol. Med.* **2,** 23–33

4. Brennan, P. A., and Zufall, F. (2006) Pheromonal communication in vertebrates. *Nature* **444,** 308–315

5. Tirindelli, R., Dibattista, M., Pifferi, S., and Menini, A. (2009) From pheromones to behavior. *Physiol. Rev.* **89,** 921–956

6. Mombaerts, P. (2004) Genes and ligands for odorant, vomeronasal and taste receptors. *Nat. Rev. Neurosci.* **5,** 263–278

7. Buck, L. B. (2000) The molecular architecture of odor and pheromone sensing in mammals. *Cell* **100,** 611–618

8. Dulac, C., and Torello, A. T. (2003) Molecular detection of pheromone signals in mammals: from genes to behaviour. *Nat. Rev. Neurosci.* **4,** 551–562

9. Leinders-Zufall, T., Ishii, T., Mombaerts, P., Zufall, F., and Boehm, T. (2009) Structural requirements for the activation of vomeronasal sensory neurons by MHC peptides. *Nat. Neurosci.* **12,** 1551–1558

10. Boehm, T., and Zufall, F. (2006) MHC peptides and the sensory evaluation of genotype. *Trends Neurosci.* **29,** 100–107

11. Boehm, T. (2006) Quality control in self/nonself discrimination. *Cell* **125,** 845–858

12. Munger, S. D., Leinders-Zufall, T., and Zufall, F. (2009) Subsystem organization of the mammalian sense of smell. *Annu. Rev. Physiol.* **71,** 115–140

13. Leinders-Zufall, T., Brennan, P., Widmayer, P., S., P. C., Maul-Pavicic, A., Jäger, M., Li, X. H., Breer, H., Zufall, F., and Boehm, T. (2004) MHC class I peptides as chemosensory signals in the vomeronasal organ. *Science* **306,** 1033–1037

14. Chamero, P., Marton, T. F., Logan, D. W., Flanagan, K., Cruz, J. R., Saghatelian, A., Cravatt, B. F., and Stowers, L. (2007) Identification of protein pheromones that promote aggressive behaviour. *Nature* **450,** 899–902

15. Kimoto, H., Haga, S., Sato, K., and Touhara, K. (2005) Sex-specific peptides from exocrine glands stimulate mouse vomeronasal sensory neurons. *Nature* **437,** 898–901

16. Ishii, T., Hirota, J., and Mombaerts, P. (2003) Combinatorial coexpression of neural and immune multigene families in mouse vomeronasal sensory neurons. *Curr. Biol.* **13,** 394–400

17. Loconto, J., Papes, F., Chang, E., Stowers, L., Jones, E. P., Takada, T., Kumánovics, A., Fischer Lindahl, K., and Dulac, C. (2003) Functional expression of murine V2R pheromone receptors involves selective association with the M10 and M1 families of MHC class Ib molecules. *Cell* **112,** 607–618

18. Liberles, S. D., Horowitz, L. F., Kuang, D., Contos, J. J., Wilson, K. L., Siltberg-Liberles, J., Liberles, D. A., and Buck, L. B. (2009) Formyl peptide receptors are candidate chemosensory receptors in the vomeronasal organ. *Proc. Natl. Acad. Sci. U.S.A.* **106,** 9842–9847

19. Rivière, S., Challet, L., Fluegge, D., Spehr, M., and Rodriguez, I. (2009) Formyl peptide receptor-like proteins are a novel family of vomeronasal chemosensors. *Nature* **459,** 574–577

20. Migeotte, I., Communi, D., and Parmentier, M. (2006) Formyl peptide receptors: a promiscuous subfamily of G protein-coupled receptors controlling immune responses. *Cytokine Growth Factor Rev.* **17,** 501–519

21. Ye, R. D., Boulay, F., Wang, J. M., Dahlgren, C., Gerard, C., Parmentier, M., Serhan, C. N., and Murphy, P. M. (2009) International Union of Basic and Clinical Pharmacology. LXXIII. Nomenclature for the formyl peptide receptor (FPR) family. *Pharmacol. Rev.* **61,** 119–161

22. Showell, H. J., Freer, R. J., Zigmond, S. H., Schiffmann, E., Aswanikumar, S., Corcoran, B., and Becker, E. L. (1976) The structure-activity relations of synthetic peptides as chemotactic factors and inducers of lysosomal secretion for neutrophils. *J. Exp. Med.* **143,** 1154–1169

23. Schiffmann, E., Corcoran, B. A., and Wahl, S. M. (1975) *N*-Formylmethionyl peptides as chemoattractants for leukocytes. *Proc. Natl. Acad. Sci. U.S.A.* **72,** 1059–1062

24. Kurosaka, K., Chen, Q., Yarovinsky, F., Oppenheim, J. J., and Yang, D. (2005) Mouse cathelin-related antimicrobial peptide chemoattracts leukocytes using formyl peptide receptor-like 1/mouse formyl peptide receptor-like 2 as the receptor and acts as an immune adjuvant. *J. Immunol.* **174,** 6257–6265

25. Ying, G., Iribarren, P., Zhou, Y., Gong, W., Zhang, N., Yu, Z. X., Le, Y., Cui, Y., and Wang, J. M. (2004) Humanin, a newly identified neuroprotective factor, uses the G protein-coupled formyl peptide receptor-like-1 as a functional receptor. *J. Immunol.* **172,** 7078–7085

26. Su, S. B., Gao, J., Gong, W., Dunlop, N. M., Murphy, P. M., Oppenheim, J. J., and Wang, J. M. (1999) T21/DP107, a synthetic leucine zipper-like domain of the HIV-1 envelope gp41, attracts and activates human phagocytes by using G-protein-coupled formyl peptide receptors. *J. Immunol.* **162,** 5924–5930

27. Fiore, S., Maddox, J. F., Perez, H. D., and Serhan, C. N. (1994) Identification of a human cDNA encoding a functional high affinity lipoxin A4 receptor. *J. Exp. Med.* **180,** 253–260

28. Chamero, P., Katsoulidou, V., Hendrix, P., Bufe, B., Roberts, R., Matsunami, H., Abramowitz, J., Birnbaumer, L., Zufall, F., and Leinders-Zufall, T. (2011) G protein Gα$_o$ is essential for vomeronasal function and aggressive behavior in mice. *Proc. Natl. Acad. Sci. U.S.A.* **108,** 12898–12903

29. Wang, Z. G., and Ye, R. D. (2002) Characterization of two new members of the formyl peptide receptor gene family from 129S6 mice. *Gene* **299,** 57–63

30. Gao, J. L., Guillabert, A., Hu, J., Le, Y., Urizar, E., Seligman, E., Fang, K. J., Yuan, X., Imbault, V., Communi, D., Wang, J. M., Parmentier, M., Murphy, P. M., and Migeotte, I. (2007) F2L, a peptide derived from heme-binding protein, chemoattracts mouse neutrophils by specifically activating Fpr2, the low-affinity *N*-formyl peptide receptor. *J. Immunol.* **178,** 1450–1456

31. Bufe, B., Hofmann, T., Krautwurst, D., Raguse, J. D., and Meyerhof, W. (2002) The human TAS2R16 receptor mediates bitter taste in response to β-glucopyranosides. *Nat. Genet.* **32,** 397–401

32. Krautwurst, D., Yau, K. W., and Reed, R. R. (1998) Identification of ligands for olfactory receptors by functional expression of a receptor library. *Cell* **95,** 917–926

33. He, R., Tan, L., Browning, D. D., Wang, J. M., and Ye, R. D. (2000) The synthetic peptide Trp-Lys-Tyr-Met-Val-D-Met is a potent chemotactic agonist for mouse formyl peptide receptor. *J. Immunol.* **165,** 4598–4605

34. Liang, T. S., Wang, J. M., Murphy, P. M., and Gao, J. L. (2000) Serum amyloid A is a chemotactic agonist at FPR2, a low-affinity *N*-formyl peptide receptor on mouse neutrophils. *Biochem. Biophys. Res. Commun.* **270,** 331–335

35. Offermanns, S., and Simon, M. I. (1995) Gα$_{15}$ and Gα$_{16}$ couple a wide variety of receptors to phospholipase C. *J. Biol. Chem.* **270,** 15175–15180

36. Mody, S. M., Ho, M. K., Joshi, S. A., and Wong, Y. H. (2000) Incorporation of Gα$_z$-specific sequence at the carboxyl terminus increases the promiscuity of Gα$_{16}$ toward G$_i$-coupled receptors. *Mol. Pharmacol.* **57,** 13–23

37. Southgate, E. L., He, R. L., Gao, J. L., Murphy, P. M., Nanamori, M., and Ye, R. D. (2008) Identification of formyl peptides from *Listeria monocytogenes* and *Staphylococcus aureus* as potent chemoattractants for mouse neutrophils. *J. Immunol.* **181,** 1429–1437

38. Martínez-Rodríguez, S., Martínez-Gómez, A. I., Rodríguez-Vico, F., Clemente-Jiménez, J. M., and Las Heras-Vázquez, F. J. (2010) Natural occurrence and industrial applications of D-amino acids: an overview. *Chem. Biodivers.* **7,** 1531–1548

39. Brandenburg, L. O., Konrad, M., Wruck, C. J., Koch, T., Lucius, R., and Pufe, T. (2010) Functional and physical interactions between formyl peptide receptors and scavenger receptor MARCO and their involvement in amyloid β$_{1-42}$-induced signal transduction in glial cells. *J. Neurochem.* **113,** 749–760

40. Partida-Sánchez, S., Cockayne, D. A., Monard, S., Jacobson, E. L., Oppenheimer, N., Garvy, B., Kusser, K., Goodrich, S., Howard, M., Harmsen, A., Randall, T. D., and Lund, F. E. (2001) Cyclic ADP-ribose production by CD38 regulates intracellular calcium release, extracellular calcium influx, and chemotaxis in neutrophils and is required for bacterial clearance *in vivo*. *Nat. Med.* **7,** 1209–1216

41. Zdobnov, E. M., von Mering, C., Letunic, I., and Bork, P. (2005) Consistency of genome-based methods in measuring Metazoan evolution. *FEBS Lett.* **579,** 3355–3361

42. Trice, J. M., and Pinals, R. S. (1985) Dimethyl sulfoxide: a review of its use in the rheumatic disorders. *Semin. Arthritis Rheum.* **15,** 45–60

43. Hartt, J. K., Liang, T., Sahagun-Ruiz, A., Wang, J. M., Gao, J. L., and Murphy, P. M. (2000) The HIV-1 cell entry inhibitor T-20 potently chemoattracts neutrophils by specifically activating the *N*-formyl peptide receptor. *Biochem. Biophys. Res. Commun.* **272,** 699–704

44. Gao, J. L., Chen, H., Filie, J. D., Kozak, C. A., and Murphy, P. M. (1998) Differential expansion of the *N*-formyl peptide receptor gene cluster in human and mouse. *Genomics* **51,** 270–276